NUMERICAL AND EXPERIMENTAL CHARACTERIZATION OF PARTICLE CLUSTERS IN RISER FLOW

A.C.VARAS, E.A.J.F.PETERS[*], N.G.DEEN, and J.A.M. KUIPERS

Department of Chemical Engineering and Chemistry, Multiphase Reactors Group, Eindhoven University of Technology, Eindhoven, THE NETHERLANDS
*Corresponding author, E-mail address: E.A.J.F.Peters@tue.nl

ABSTRACT

A numerical and experimental study of riser hydrodynamics is performed under fast fluidization regime conditions. The measured data sets are used for validation of CFD-DEM simulations. Special attention is paid to the formation of heterogeneities in the particle distribution, i.e., the formation of clusters. Particle Image Velocimetry (PIV) in combination with Digital Image Analysis (DIA), provides a complete data set for the particle flow in a pseudo-2D riser reactor. A novel DIA post-processing technique is used to measure the solids volume fraction. A CFD-DEM model is employed to simulate the co-current gas-particle flow. Particle clusters are detected in both, experiments and simulations, by applying the Sharma criteria. Core-annulus flow is well predicted by the model and other hydrodynamic parameters were also in good agreement with experimental values.

NOMENCLATURE

c	pixels per particle diameter, pixels/m
d_p	particle diameter, m
$\bar{F}_c$	particle collision force, N
$\langle \bar{G}_s \rangle$	time-averaged solids mass flux, kg/m²s
I_{2D}	normalized 2D intensity
I_p	moment of inertia, N m
m	mass, kg
P	pressure, Pa
$\bar{r}$	position vector, m
$\bar{s}_p$	solids displacement vector, m
$\bar{S}_p$	momentum source term, N/m³
$\bar{T}_p$	torque force, N m
Δt_{Exp}	time between two consecutive frames, s
Δt_{Gas}	gas phase time step, s
Δt_{DEM}	particle phase time step, s
$\bar{u}$	gas velocity vector, m/s
$\bar{v}_p$	particle velocity vector, m/s
V	volume, m³
w	image contrast, intensity counts
x/W	riser width, (-)
Δz	depth of pseudo 2D domain, m
β	interphase momentum transfer coefficient, kg/m³s
ε	porosity m³gas/m³reactor
ρ_g	gas density, kg/m³
μ	dynamic viscosity, kg/m s
$\bar{\bar{\tau}}$	stress tensor, Pa
φ_{3D}	solids volume fraction m³solid/m³reactor
ω_p	particle rotational velocity, 1/s

INTRODUCTION

Riser reactors are fluidized systems where typically gas and solid phases interact to carry out chemical processes that need high mixing rates and short gas residence times. The hydrodynamic behavior of risers is characterized by high gas superficial velocities and a controlled solids feeding. Both parameters are regulated according to the needs of the process. Fast fluidization regimes are characterized by a very dilute region in the core of the reactor, while denser areas are found close to the wall, forming groups of particles or clusters. This is the so called core-annulus flow structure.

The formation of particle clusters influences the mass transfer between the gas and the solids that takes place in the riser. For instance, in a high temperature catalytic reaction, the solid-gas contact efficiency could be significantly diminished in regions with clusters, due to the lower gas accessibility to particles that are inside the cluster. Thus, the performance of riser reactors is negatively affected by the presence of these clusters.

The presence of particle clusters is heavily influenced by inelastic collisions of particles with each other and the reactor walls. By combining experiments and simulation we want to obtain a quantitative insight in the mechanisms of cluster formation. The first step is to compare experimental results with predictions of CFD-DEM simulations.

Numerous works have characterized riser hydrodynamics and reported cluster-related properties such as internal porosity, size, aspect ratio or cluster frequency (Cabezas-Gómez et al. 2008; Tsuo and Gidaspow 1990; Horio and Kuroki 1994; Guenther and Breault 2007). One difficulty is how to define a particle cluster in a systematic way. In this paper we use Soong's criterion, which was further complemented by Sharma et al. (Sharma et al. 2000). Although these criteria could be by some means arbitrary (Cabezas-Gómez et al. 2008), they have been employed by several authors to systematically detect clusters (Capecelatro, Pepiot, and Desjardins 2014; Cabezas-Gómez et al. 2008; Sharma et al. 2000; Li et al. 2011; Manyele, Pärssinen, and Zhu 2002; Harris, Davidson, and Thorpe 2002).

Nowadays, there are non-intrusive techniques that allow the measurement of hydrodynamic parameters of the whole system field, such as Magnetic Resonance Imaging, Electrical Capacitance Tomography and the combination of Particle Image Velocimetry (PIV) and Digital Image Analysis (DIA). In this work, a novel 'temporally-histogram' based DIA method is applied to measure the

solids volume fraction in a pseudo-2D riser reactor. This method provides accurate solids volume fraction measurements over the whole system field. The combined PIV/DIA technique supplies not only solids volume fraction and particles motion data, but also cluster-related properties that characterize the hydrodynamics of a fast fluidized bed.

Concerning numerical works related to cluster phenomena, Euler-Euler as well as Euler-Lagrange models have been employed to predict the hydrodynamic behavior of riser reactors. Energy dissipation models have been employed to further describe the clusters motion in continuum models (Shuai et al. 2012; Zhou and Wang 2015), where the scale of resolution is considerably bigger than the typical size of particle structures formed at mesoscale levels.

Numerous researchers have previously reported experimental and computational works about cluster-related phenomena (Capecelatro, Pepiot, and Desjardins 2014; Ouyang and Li 1999; Lackermeier et al. 2001; Horio and Kuroki 1994). However, little work is found on quantitative comparison of cluster properties between simulations and experiments. Shuai et al. 2012, Helland et al. 2007 used cluster-dependent drag correlations to describe cluster phenomena.

CFD-DEM models describe the motion of particles as discrete elements and capture well the formation of clusters (Johansen et al. 2010). Riser hydrodynamics and clustering formation are significantly affected by the collision properties of the solid phase (Hoomans et al. 1996). The riser hydrodynamics are also significantly affected by the collision parameters and the different drag correlations that have been investigated over the last years (Beetstra, van der Hoef, and Kuipers 2007)

In this article, a CFD-DEM method is utilized to predict the hydrodynamics in the pseudo-2D riser. The same operational conditions of superficial gas velocity and solids mass flux are used as for the PIV/DIA experiments. A detailed comparison between experimental and simulation data sets will be presented.

MODEL DESCRIPTION

CFD-DEM Model

A Discrete Element Model was employed to perform simulations of a pseudo-2D riser reactor (Deen et al. 2007). Navier Stokes equations are solved to describe the fluid dynamics of the gas phase by means of a finite difference method:

$$\frac{\partial(\varepsilon\rho_g)}{\partial t} + \nabla\cdot\left(\varepsilon\rho_g\bar{u}\right) = 0 \qquad (1)$$

$$\frac{\partial(\varepsilon\rho_g\bar{u})}{\partial t} + \nabla\cdot\left(\varepsilon\rho_g\bar{u}\bar{u}\right) = -\varepsilon\nabla P - \nabla\cdot(\varepsilon\bar{\bar{\tau}})$$
$$-\bar{S}_p + \varepsilon\rho_g\bar{g} \qquad (2)$$

The gas and solids motion is coupled via a sink term that represents the two-way coupling:

$$\bar{S}_p = \frac{1}{V_{cell}}\sum_{i=0}^{Np}\frac{\beta V_p}{1-\varepsilon}\left(\bar{u} - \bar{v}_p\right)D\left(\bar{r} - \bar{r}_p\right) \qquad (3)$$

Here $D\left(\bar{r} - \bar{r}_p\right)$ is a distribution function that smoothens the exerted force at the particle positions to provide the source term for the un-resolved gas phase hydrodynamics.

The particle motion is governed by the Newtonian equations of motion:

$$m_p\frac{d^2\bar{r}_p}{dt^2} = -V_i\nabla P + \frac{\beta V_p}{1-\varepsilon}\left(\bar{u} - \bar{v}_p\right) + m_p\bar{g} + \bar{F}_c \qquad (4)$$

$$I_p\frac{d\omega_p}{dt} = \bar{T}_p \qquad (5)$$

The particle collision forces are computed by means of a soft sphere model that was firstly reported by (Cundall and Strack 1980).

PIV - DIA EXPERIMENTAL TECHNIQUE

PIV

Particle Image Velocimetry is used to measure the particles velocity between two consecutive frames. The raw images are subdivided into interrogation areas. By means of image cross-correlation, the displacement vector $\bar{s}_p(\bar{x},t)$ of the particle phase is computed. Thus, the particle velocity can be expressed as follows:

$$\bar{v}_p(\bar{x},t) = \frac{\bar{s}_p(\bar{x},t)}{\Delta t_{Exp}} \qquad (6)$$

where Δt_{Exp} is the time difference between the two consecutive frames. The experiments were performed in a pseudo-2D riser reactor where the recordings were made with a high resolution camera (2016×2016 pixel).
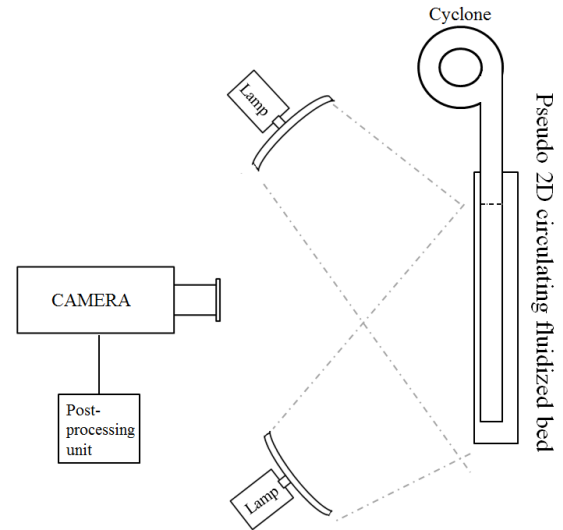
Figure 1: Top view of experimental setup.

The dimensions of the pseudo-2D riser are 1.5×0.07×0.006 m. It has a lateral top outlet coupled to a cyclone, where gas and particles are separated. 0.8 mm glass beads were fed to the bottom of the riser from a downer that was fluidized at velocities close to u_{mf}. The solids mass flux is regulated by a small opening in the recycling pipe of the system.

Novel DIA Post-processing Method

A novel post-processing DIA algorithm has been developed. We named this the 'temporal histogram method' (THM), because it first builds an intensity histogram for each pixel using all intensity values that are experienced by that pixel during a recording. In the next step this information is used to normalize the 2D intensity field such that effects like uneven lighting and background irregularities are eliminated.

After averaging the 2D intensity over an interrogation window, the normalized 2D intensity can be correlated to the 3D solids volume fraction via the following functional form:

$$\varphi_{3D} = A \cdot B \cdot \operatorname{atanh}\left(\frac{I_{2D}}{A}\right) \qquad (7)$$

The constants A and B in this equation depend on the image contrast and resolution, the ratio of the particle diameter and the bed depth.

The dependencies of A and B are obtained from synthetic images that were generated from CFD-DEM simulations. Clearly, in simulations φ_{3D} is known. We therefore use simulation data to render images that closely resemble experimental images. That is, besides rendering the particles using particle radii and positions from the CFD-DEM simulations, we also included uneven lighting, background irregularities, shadows, noise etc. After post-processing these synthetic images using THM we obtained I_{2D} in addition to the already known φ_{3D}. These data-sets were used subsequently to fit the A and B parameters.

This calibration was performed under different imaging conditions showing that this technique is very stable under strong changes in the image contrast and resolution(quantified in pixels per particle diameter). One of the big advantages of this method is that the solids fraction quantification is based on image-related properties and does not need any calibration with the solids weight of the system, which is constantly changing under riser flow conditions.

The dependencies for A and B we found in this way are expressed in eqns. (8) and (9):

$$A = 0.99 \pm 0.01 \qquad (8)$$

$$B\left(\frac{d_p}{\Delta z}\right) = 0.6818 \cdot d_p/D + 0.024 \pm 0.001 \qquad (9)$$

where d_p is the particle diameter and Δz the bed depth.

Thus, the combined PIV-DIA method is applied to collect large data sets of solids volume fraction and solids velocity, and enables the quantification of solids mass flux. Instantaneous solids fraction and solids velocity data are used to compute the time-averaged axial solids mass flux G_s, at each interrogation area:

$$\langle \bar{G}_s \rangle = \rho_s \langle \varphi_{3D}(x,t) \cdot \bar{v}_p(x,t) \rangle \qquad (10)$$

Each experiment consisted of 4990 images, covering a total duration of 50 seconds.

SIMULATIONS

A top side outlet was incorporated in the simulation domain to take into account the influence of the lateral outlet of the system. No-slip boundary conditions were applied to the gas phase at the top, front, back and right walls, while a prescribed inflow velocity was applied to the bottom. The left side wall was subdivided into two regions, a top-left region of 0.07 m with prescribed pressure, and below this point no-slip boundary conditions were set as Figure 2 illustrates.
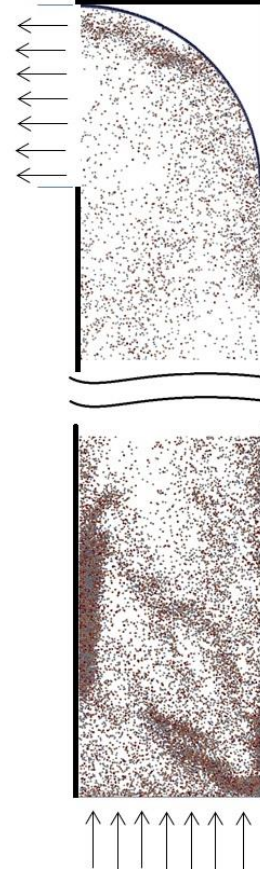
Figure 2: Snapshot of pseudo-2D riser in CFD-DEM model.

Particles were introduced from bottom X-Y plane of the simulation domain at a z-coordinate between 0 and 3 times the particle radius at random x and y positions. At the top a curved wall consisting of 1 mm stationary particles was inserted to render a lateral outlet like in the experiments. The particles were leaving the domain at the top-left side outlet, mimicking in this way the side outlet of the experimental unit.

The normal and the tangential restitution coefficient between particles (glass beads) were 0.96 and 0.33, respectively, while the restitution coefficient between the glass beads of the system and the walls, including the particulate wall, was 0.86 (Hoomans et al. 1996). Additional simulation parameters are specified in Table 1.

In Figure 2, a snapshot of the pseudo-2D riser is shown. The curved blue wall at the top of the domain delimits the side outlet of the riser. The total simulation time was 15 seconds. In the post-processing the first 1.5 seconds were neglected to not account for the initialization stage. Beyond that simulation time, steady state was assumed.

NX	28	d_p(mm)	0.8-0.9
NY	5	ρ_s(kg/m^3)	2500
NZ	628	μ_g (kg/ms)	$1.8 \cdot 10^{-5}$
X (m)	0.07	T (K)	298
Y (m)	0.006	$e_{p\text{-}p}$	0.96
Z (m)	1.57	e_t	0.33
Δt_{Gas} (s)	$5.0 \cdot 10^{-5}$	$e_{p\text{-}w}$	0.86
Δt_{DEM} (s)	$5.0 \cdot 10^{-6}$	μ_{fr}	0.15
G_s (kg/m^{2}s)	32.9	k_n(N/m)	1600
U (m/s)	5.95	P	1 atm

Table 1: Simulation Parameters.

Simulation data were obtained each 0.005 seconds. Post-processing of these data was performed to mimic the cluster detection method similar to the one in experiments (see below).

Cluster Detection

Clusters have been detected according to Soong's and Sharma's criteria (Sharma et al. 2000). They defined a cluster as a group of particles with internal solids fraction above $\langle \varepsilon_s \rangle + 2\sigma$, (where the averaged solids fraction fluctuations is $\sigma^2 = \langle (\varepsilon_s - \langle \varepsilon_s \rangle)^2 \rangle$). These groups of particles should also be at least of one or two orders of magnitude bigger than the particle diameter.
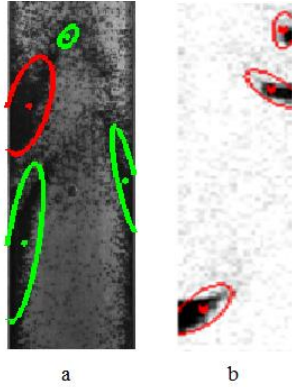
Figure 3: Detected clusters. a) Experimental image b) Solids fraction field of CFD-DEM simulation.

Thus, in our case all groups of grids or interrogation areas that were bigger than 8 mm and had an internal solids fraction above $\langle \varepsilon_s \rangle + 2\sigma$ were considered as particle clusters. The detection of clusters was performed by post-processing experimental recordings and simulation data by means of a Matlab ® script.

The cluster projected area was calculated by evaluating the number of grids that were occupied by a cluster. Clusters with an area smaller than $5.02 \cdot 10^{-5}$ m^2 (corresponding to a circular area of 8 mm diameter) were neglected.

The combination of PIV-DIA enables the quantification of several cluster-related properties such as: mass, aspect ratio, diameter as well as cluster velocity. In Figure 3, clusters can be observed in both experiments and simulations. Green ellipses correspond to clusters moving upwards, while red ones move downwards. It is noted that dense clusters are formed close to the wall and tend to fall down, while big dilute strands of particles tend to move upwards.

RESULTS AND DISCUSSION

In this section we will present results for one parameter set as given in Table 1.

Time-averaged Solids Fraction

Since the local solids volume fraction has been used as a primary criterion to detect clusters, this will be the first parameter to analyze.

In Figure 4, the time-averaged axial solids volume fraction profile is shown. The most obvious conclusion that can be drawn from these results is that the riser system is more dilute at higher positions than in the bottom of the riser. The time-averaged axial solids volume fraction profile, which is spatially averaged, is gradually decreasing along the axial direction in, both, experimental and computational cases.
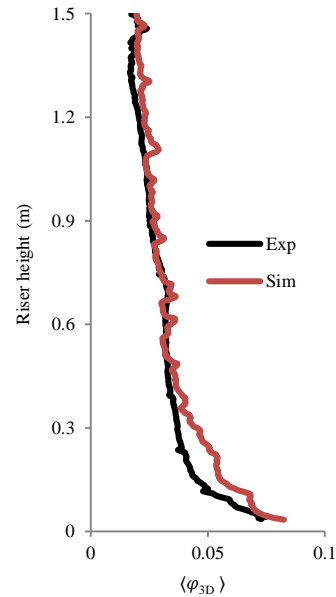
Figure 4: Time-averaged axial solids fraction profile.

Although Figure 4 shows a good correspondence between simulations and experiments in terms of magnitude and shape, it can be seen that the simulations slightly overestimate the solids fraction of the system throughout the whole axial domain. In the simulation data, some fluctuations are observed. This is most probably due to formation of clusters at these axial coordinates that locally increase the solids fraction. The cluster formation probability is less frequent at higher positions in the riser. Since the simulation time is 15 seconds and the cluster frequency is relatively low at the highest axial coordinates, the punctual formation of clusters can result in fluctuations even for the time-averaged data.

Figure 5 shows the results of the cross-sectional solids fraction profiles at three different heights. The profiles are U-shaped, describing well the core-annulus behavior. It is noted that, in experiments, near the bottom regions there is a small asymmetry in the profile, probably due to the lateral solids inlet at the bottom of the riser. In the simulations, a uniform solids inlet is simulated, which could explain the observed difference. While, at z=0.82 m the correspondence is good, at z=1.41 m, more asymmetry is found in the simulation results. The profile is considerably denser at the right side of the domain than the left side (where the side outlet is placed). This effect is

not observed in the experimental results, which profiles are symmetric except at the lowest axial profile, where the influence of the lateral solids inlet could have an effect.
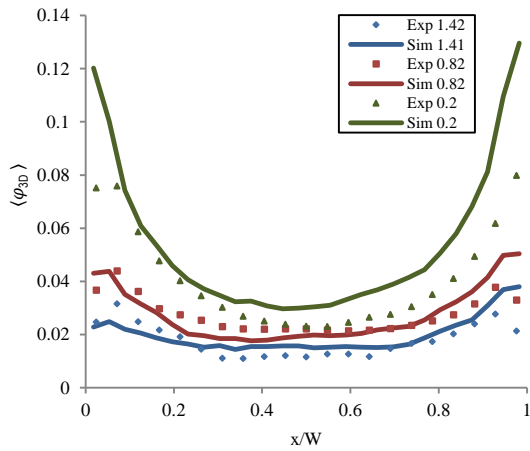
Figure 5: Cross-sectional profiles of time-averaged solids volume fraction at three different heights.

Although the shape of the profiles are slightly different, we conclude that the solids volume fraction is well predicted by the model in terms of magnitude.

Solids Mass Flux

In Figure 6, computational and experimental results of the time –averaged solids mass flux are plotted. It can be seen that the asymmetry in simulations is much more pronounced than in experiments, especially at higher points of the simulation domain.

In simulations, the particles flow upwards in the core of the domain and downwards close to the walls. However, the closer to the top outlet, the bigger the asymmetry between left and right in the profile is found to be. At z=1.41 the simulations predict a net solids upflow of particles on the outlet side, while at the closed side there would be a significant solids downflow probably due to particle collisions with the top curved wall. This phenomenon could enhance the solids downflow of particles on the right side of the domain, promoting a higher cluster formation frequency, as it will be further discussed in the next subsection.

This asymmetry is not found in the experimental measurements. A possible cause can be that the (effective) collisional properties in the simulations are not realistic.

The collision properties between the particles of the system and the particles that were used to build the curved top-section are those corresponding to polished stainless-steel and glass. However, the curved wall (being made up of particles) presents a rough surface. This roughness might influence the collisions of the particles and have a large effect on the solids flux profile in the top section. This needs further investigation.

Cluster Count

As explained, clusters were systematically detected by applying Soong and Sharma criteria.

The center of mass of each cluster was located in the riser domain. It has to be noted that the total number of detected clusters does not correspond to the total number of clusters

that are formed in an experiment or simulation, since the cluster formation is not specifically tracked. In other words, the total number of clusters would not be a representative property of the system heterogeneity, since a cluster could be present in multiple frames. Thus, the total number of clusters are normalized by the corresponding number of images or input files, conveying a static property of the system.
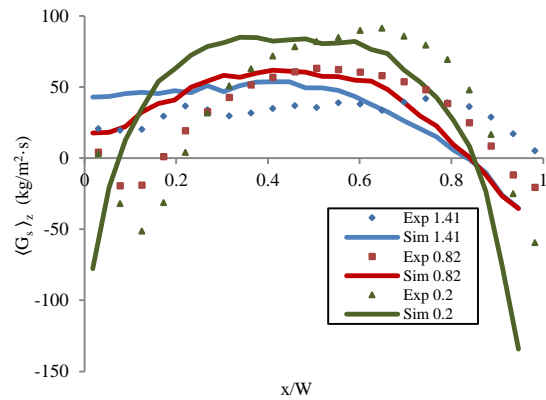
Figure 6: Cross-sectional profiles of axial solids mass flux.
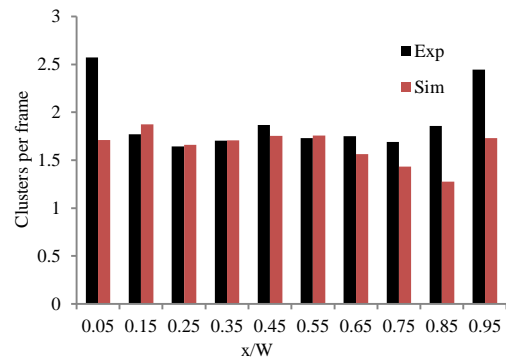
Figure 7: Clusters per frame vs riser width.

The center of mass of all detected clusters are binned throughout the width of the riser reactor. In Figure 7, the number of clusters per frame in each one of these bins are plotted. The frequency of cluster events corresponds well with experiments in terms of magnitude. However, it can be noticed from the experimental results that the cluster events are more frequent close to the walls than in the core of the reactor, providing another evidence of the core-annulus behavior that takes place in the riser. Whereas the computational data show a lower cluster frequency than in the simulations. This is consistent with the asymmetries observed for the solids volume fraction and solids mass flux profiles.

By any means, the E-L model provides a relatively accurate estimation of the clustering frequency of the real experiment.

The projected cluster area was also quantified in an attempt to further characterize the clusters that were formed in the system. The number of grids occupied by a cluster were used to estimate their corresponding projected area.

5
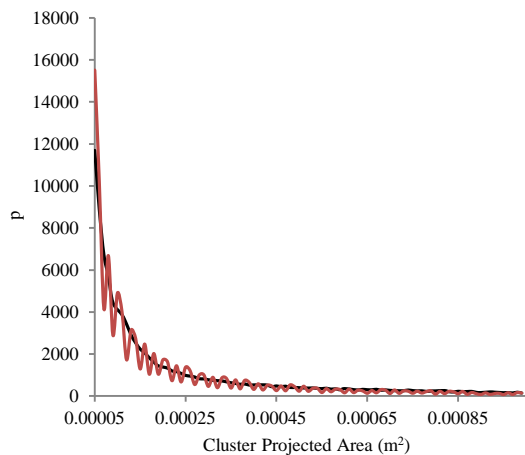
Figure 8: Probability distribution of cluster projected area.
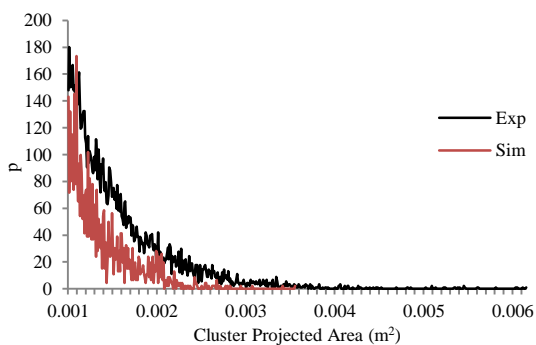
Figure 9: Zoom in of cluster area probability distribution function focusing on large cluster sizes.

In Figure 8 shows the probability distribution function of the cluster area. Clusters with smaller area than $5.02 \cdot 10^{-5}$ m^2 were neglected.

It is shown, that the cluster size distribution is well predicted by the model. In Figure 9, the zoomed-in plot of the size distribution function shows that in experiments bigger clusters are formed than in simulations. This underestimation of big clusters is balanced with a slight overestimation of smaller clusters, as Figure 8 illustrates.

CONCLUSIONS

CFD-DEM is shown to describe well the core-annulus behavior of fast fluidized systems. An overall good correspondence with experiments has been obtained in terms of solids volume fraction and cluster count per frame. The probability distribution function of the projected cluster area was also in relatively good correspondence.

Although the solids inventory were quantitatively similar in simulations and experiments, solids mass flux profiles show a different behavior of the solid phase, which motion is particularly affected by the incorporated top outlet in the simulations. The results show that in the experimental unit these profiles are relatively uniform, while in simulations, a strong particle downflow prevails.

With respect to clusters it was found that the number of big clusters, with areas above 1.0×10^{-3} m^2, was sensitively underestimated by the simulations.

These findings suggest that Euler-Lagrange models can provide accurate results for riser hydrodynamics and particle cluster characterization. However, further research is recommended on the study of collision parameters, especially with the walls of the simulation domain that have a great influence on the solids motion. Ongoing work is being carried out to further analyze the influence of operational riser conditions on the experimental cluster characterization and its computational prediction by CFD-DEM modelling.

REFERENCES

BEETSTRA, R., M.A. VAN DER HOEF, and J.A.M. KUIPERS. 2007. "Numerical Study of Segregation Using a New Drag Force Correlation for Polydisperse Systems Derived from Lattice-Boltzmann Simulations." Chemical Engineering Science 62 (1-2): 246–55. doi:10.1016/j.ces.2006.08.054.

CABEZAS-GÓMEZ, L., R. C. DA SILVA, HÉLIO A. NAVARRO, and F. E. MILIOLI. 2008. "Cluster Identification and Characterization in the Riser of a Circulating Fluidized Bed from Numerical Simulation Results." Applied Mathematical Modelling 32 (3): 327–40. doi:10.1016/j.apm.2006.12.005.

CAPECELATRO, J., P. PEPIOT, and O. DESJARDINS. 2014. "Numerical Characterization and Modeling of Particle Clustering in Wall-Bounded Vertical Risers." Chemical Engineering Journal 245. Elsevier B.V.: 295–310. doi:10.1016/j.cej.2014.02.040.

CUNDALL, P. A., and O. D. L. STRACK. 1980. "Discussion: A Discrete Numerical Model for Granular Assemblies."Géotechnique.doi:10.1680/geot.1980.30.3.331.

DEEN, N.G., M. VAN SINT ANNALAND, M.A. VAN DER HOEF, and J.A.M. KUIPERS. 2007. "Review of Discrete Particle Modeling of Fluidized Beds." Chemical Engineering Science 62 (1-2): 28–44. doi:10.1016/j.ces.2006.08.014.

GUENTHER, C., and R. BREAULT. 2007. "Wavelet Analysis to Characterize Cluster Dynamics in a Circulating Fluidized Bed." Powder Technology 173: 163–73. doi:10.1016/j.powtec.2006.12.016.

HARRIS, A. T., J. F. DAVIDSON, and R. B. THORPE. 2002. "The Prediction of Particle Cluster Properties in the near Wall Region of a Vertical Riser (200157)." Powder Technology 127 (2): 128–43. doi:10.1016/S0032-5910(02)00114-6.

HOOMANS, B.P.B., J.A.M. KUIPERS, W.J. BRIELS, and W.P.M. VAN SWAAIJ. 1996. "Discrete Particle Simulation of Bubble and Slug Formation in a Two-Dimensional Gas-Fluidised Bed: A Hard-Sphere Approach." Chemical Engineering Science 51 (1): 99–118. doi:10.1016/0009-2509(95)00271-5.

HORIO, M., and H. KUROKI. 1994. "Three-Dimensional Flow Visualization of Dilutely Dispersed Solids in Bubbling and Circulating Fluidized Beds." Chemical Engineering Science 49 (15): 2413–21. doi:10.1016/0009-2509(94)E0071-W.

JOHANSEN, S, M BRAUN, B POPOFF, and S AMINI. 2010. "Evaluation of a Lagrangian Discrete Phase

Modeling Approach for Resolving Cluster Formation in CFB Risers," no. June 2015: 1–8.

LACKERMEIER, U., C. RUDNICK, J. WERTHER, A. BREDEBUSCH, and H. BURKHARDT. 2001. "Visualization of Flow Structures inside a Circulating Fluidized Bed by Means of Laser Sheet and Image Processing." Powder Technology 114: 71–83. doi:10.1016/S0032-5910(00)00265-5.

LI, D., J. ZHU, M. B. RAY, and A. K. RAY. 2011. "Catalytic Reaction in a Circulating Fluidized Bed Downer: Ozone Decomposition." Chemical Engineering Science 66 (20). Elsevier: 4615–23. doi:10.1016/j.ces.2011.06.027.

MANYELE, S. V., J. H. PÄRSSINEN, and J. X. ZHU. 2002. "Characterizing Particle Aggregates in a High-Density and High-Flux CFB Riser." Chemical Engineering Journal 88: 151–61. doi:10.1016/S1385-8947(01)00299-6.

OUYANG, J., and J. LI. 1999. "Discrete Simulations of Heterogeneous Structure and Dynamic Behavior in Gas–solid Fluidization." Chemical Engineering Science 54: 5427–40. doi:10.1016/S0009-2509(99)00275-4.

SHARMA, A. K., K. TUZLA, J. MATSEN, and J. C. CHEN. 2000. "Parametric Effects of Particle Size and Gas Velocity on Cluster Characteristics in Fast Fluidized Beds." Powder Technology 111: 114–22. doi:10.1016/S0032-5910(00)00247-3.

SHUAI, W., L. GUODONG, L. HUILIN, X. PENGFEI, Y. YUNCHAO, and D. GIDASPOW. 2012. "A Cluster Structure-Dependent Drag Coefficient Model Applied to Risers." Powder Technology 225. Elsevier B.V.: 176–89. doi:10.1016/j.powtec.2012.04.006.

TSUO, Y. P. and D. GIDASPOW. 1990. "Computation of Flow Patterns in Circulating Fluidized Beds." AIChE Journal 36 (6): 885–96. doi:10.1002/aic.690360610.

ZHOU, Q., and J. WANG. 2015. "CFD Study of Mixing and Segregation in CFB Risers: Extension of EMMS Drag Model to Binary Gas–solid Flow." Chemical Engineering Science 122 (January). Elsevier: 637–51. doi:10.1016/j.ces.2014.10.025.